J Solid State Electrochem (2014) 18:2267–2277
DOI 10.1007/s10008-014-2477-0

ORIGINAL PAPER

Electrochemical behavior of silver thin films interfaced with yttria-stabilized zirconia

Michèle Fee · Spyridon Ntais · Arnaud Weck · Elena A. Baranova

Received: 22 January 2014 / Revised: 2 April 2014 / Accepted: 7 April 2014 / Published online: 23 April 2014

Abstract Thin silver films (100–800 nm) were deposited by physical vapor deposition (PVD) on yttria-stabilized zirconia solid electrolyte. The electric percolation as a function of the film thickness was studied during deposition and annealing using a two-electrode in-situ resistance measurement technique. Electrical percolation was achieved in as-deposited films greater than 5.4±0.4 nm; however, thermal treatment (550 °C in air) resulted in film dewetting for Ag films as thick as 500 nm and formation of electronically isolated Ag nanoparticles, as was confirmed by SEM and XPS. In thermally treated samples, stable electronic conductivity associated with a continuous percolated network was only observed in samples greater than 600 nm in thickness. The effect of polarization on the electrochemical reactions at the three-phase (electrode-gas-electrolyte) and two-phase (electrode-electrolyte) boundaries of the electrode was investigated by solid electrolyte cyclic voltammetry (SECV) at 350 °C and P_{O2}=6 kPa. With the application of positive potential, silver oxide (Ag_2O) was found to form along the three-phase boundary and then extends within the bulk of the electrode with increasing anodic potentials. By changing the hold time at positive potential, passivating oxide layers are formed which results in a shift in favor of the oxygen evolution reaction at the working electrode. This oxide forms according to a logarithmic rate expression with thick oxides being associated with decrease in current efficiency for subsequent oxide formation.

M. Fee · S. Ntais · E. A. Baranova (✉)
Department of Chemical and Biological Engineering, Centre for Catalysis Research and Innovation (CCRI), University of Ottawa, 161 Louis Pasteur, Ottawa, ON K1N 6N5, Canada
e-mail: elena.baranova@uottawa.ca

A. Weck
Department of Mechanical Engineering, University of Ottawa, 161 Louis Pasteur, Ottawa, ON K1N 6N5, Canada

Keywords Silver · Thin film · PVD · Yttria-stabilized zirconia · Cyclic voltammetry · Percolation

Introduction

Stabilized zirconias are O^{2-} conductors often used as a solid electrolyte in solid oxide fuel cells (SOFC) [1], solid electrolyte membrane reactors [2], gas sensors [3], electrochemical promotion of catalysts (EPOC) [4–6], and as a support material in heterogeneous catalysis for a variety of reaction systems [6–10]. Yttria is a common stabilizing species which yields a mechanically and thermally stable cubic fluorite structured ceramic with full stabilization and maximum conductivity occurring at yttria contents between 8 and 15 mol % [11]. Silver deposited on yttria-stabilized zirconia (YSZ) has been studied as a potential cathode material in SOFCs due to its high catalytic activity and high oxygen solubility [12]. Unfortunately, due to the low melting point and high volatility of silver, applications with temperatures greater than 850 °C are not suited to the thermally unstable silver films [13]. As a result, intermediate temperature (ca. 200–550 °C) applications such as micro-solid oxide fuel cells featuring silver have been studied [1]. In addition to the studied electrochemical behavior, silver has shown interesting catalytic activity for the epoxidation of ethylene [14–17], selective reduction of NO_x [18], hydrogenation of CO_2 [19], and methane oxidation [20] reactions at intermediate temperatures (200–600 °C). Another promising application of silver film electrode-catalyst is in EPOC [21–23]. This is a catalytic phenomenon which occurs in metal or metal oxide electrode-catalysts interfaced with solid electrolytes. With the polarization of the catalyst-electrode using small currents (μA) or electrical potentials (±2 V), a pronounced and reversible modification of catalytic behavior has been observed as a result of the electrochemical back-spillover of conducted ions from the support into or from

the catalysts [24]. Catalytic materials found to exhibit this behavior under polarization must be electronically conductive and show some intrinsic open-circuit catalytic activity [24]. Because EPOC combines electrochemical and catalytic processes at the interfaces, the study of the catalyst behavior under polarization has been carried out for several systems using solid electrolyte cyclic voltammetry (SECV) [26–30]. This technique, first developed by Wagner [25], was applied by Vayenas et al. [26] as a useful tool in studying the solid electrolyte and catalyst interfaces of EPOC systems, as well as the three-phase boundary (tpb) between solid electrolyte, catalyst, and the gas phase. It was shown [26] that a measure of the quantity and location of electrochemically formed oxides resulting from the back-spillover of O^{2-} species from the support can be determined through the application of sweeping electrical potentials. At intermediate temperatures (290–575 °C), this technique has been applied to investigate the electrochemical behavior of thick platinum electrodes (5–10 μm) prepared using Pt paste (Engelhard A1121) [26], thin platinum (880 nm) [27, 28], and nickel (880 nm) [29] films deposited by sputtering and recently a thermally decomposed Pd film [30] interfaced with YSZ. However, since the low control of the microstructure and in some cases the film composition of paste electrodes may impact the results of mechanistic studies [31], the use of physical vapor deposition (PVD) techniques shows a great advantage for synthesis of metal films of controlled thickness, structure, and composition [31].

In this work, the detailed study of the electrochemical behavior of a silver, thin film (800 nm) deposited on YSZ (Ag/YSZ) using evaporative PVD technique is carried out. To this end, the cyclic voltammetry (CV) of Ag/YSZ was performed by varying the CV conditions, such as the initial positive potential of the CV, the hold time at the anodic potential, and CV scan rate. Based on the experimental results, the mechanism of formation and location of electrochemically controlled silver oxides is proposed.

Experimental

Preparation of samples

Preparation of YSZ solid-electrolyte disc

YSZ discs were synthesized by pressing and sintering commercial co-precipitated 8 mol% Y_2O_3–ZrO_2 powder (TOSOH-8Y). Powders were placed in a stainless steel die and pressed at 5,000 psi. This disc was heated in a CARBOLITE chamber furnace on a zirconia plate at 1,000 °C for 1 h followed by 1,500 °C for 6 h with ramps of 10 °C min^{-1}. The resulting polycrystalline discs measured, 1 × 18 mm, having densities of greater than 98 % the theoretical maximum density and had an ionic conductivity at 350 °C of 1.6±0.2 μS cm^{-1} as measured using Electrochemical Impedance Spectroscopy (EIS). The discs were cleaned by sonication in acetone (10 min), deionized water (18 MΩ cm^{-1}) (10 min), and isopropanol (10 min) and then allowed to dry completely in air.

Deposition of Ag film-electrode

Silver films were deposited into cleaned YSZ disks using evaporative PVD (BOC Auto306) with resistive heating of tungsten dimple boats (Kurt J. Lesker) at 2.5×10^{-5} mBar. Silver slugs (99.99 % metal basis, Alpha Aesar) were heated in a tungsten boat by the application of an electrical current of 4.5 A until a deposition rate of 0.5 nm s^{-1} was achieved as measured in-situ with a quartz microbalance thin film monitor (Edwards, FTM-5). An 800 nm silver film was produced for cyclic voltammetry studies. For percolation threshold measurement found in "Percolation studies of silver films", silver films with five different thicknesses (100, 370, 500, 600, and 800 nm) were prepared on YSZ discs.

Preparation of the electrochemical cell

The 800-nm silver film was deposited with a geometric surface area of 2.5 cm^2 using a circular mask. Counter (geometric area≈2.46 cm^2) and pseudo-reference (geometric area≈0.2 cm^2) gold electrodes were painted into the opposite side of YSZ according to the configuration shown in elsewhere [32]. Gold wires were connected to the electrodes with gold paste (Gwent). These wires were anchored with high temperature ceramic paste (Aremco, Ultra-Temp 516) into uncoated segments of the pellet. The cement and gold paste were cured at 550 °C for 1 h in air.

Characterization

SEM

Scanning electron microscopy (SEM) was used to observe changes in morphology of 100 and 800-nm-thin Ag films as a result of elevated temperatures and polarization. Imaging was performed with a JSM-7500F FESEM (JEOL) in lower secondary electron image (LEI) mode with an acceleration voltage of 1 kV, an emission current of 20 μA and working distance of 9 mm.

Percolation measurements of Ag film

Measurement of the film thickness dependence on thermal stability of silver thin films on YSZ was determined using in-situ resistance measurements. Silver films were

deposited on YSZ disk to thicknesses of 100, 370, 500, and 600 nm with a deposition rate of 0.5 nm s^{-1} and at a pressure of 2.5×10^{-5} mBar. Two electrical connections to the film were made with gold wires (99.9 % metal basis, ø=0.3 mm, Alfa Aesar) and small NiCr (80 % Ni, 20 % Cr, Omega Engineering Inc.) clips were used to make a contact between Ag film and Au wire. A K-type thermocouple was fixed in the close vicinity to the Ag film. Percolation measurements were carried out in a 200 mL CSTR-type quartz reactor. A gas mixture consisting of helium (4.7 grade, Linde) and oxygen (4.7 grade, Linde) was achieved using MKS 1359C mass flow controllers. The films were treated at 550 °C in air for the first hour to simulate the pretreatment used in SECV studies and then cooled to the operating temperature of 350 °C in P_{O_2} =6 kPa (F_{TOT}=50 mL min^{-1}) with a balance of He. The film resistances were measured with an Agilent U1271A data logging multi-meter.

XPS

The X-ray photoelectron spectroscopy (XPS) analysis was conducted on a KRATOS Axis Ultra DLD with a Hybrid lens mode at 140 W and pass energy 20 eV using a monochromatic AlKα (E=1,486.6 eV). In all cases, the operating pressure in the analysis chamber was less than 1×10^{-9} mbar. The deconvolution of the Ag3d peaks was performed using peaks with spin orbit splitting 6 eV, respectively, and with an intensity ratio $I_{3d_{5/2}}/I_{3d_{3/2}} = 1.5$ [33]. The binding energy (BE) scale was corrected using the C1s peak at 284.6 eV as an internal standard. The accuracy of measurement of the binding energy was ±0.1 eV while that of FWHM was ±0.05 eV.

Electrochemical measurements

The electrochemical cell described in 2.1.3 was placed in a 200 mL CSTR-type reactor made of Pyrex® as shown elsewhere [27]. Helium (99.997 %, Linde) and oxygen (99.997 %, Linde) gases were mixed with MKS 1359C mass flow controllers to achieve a total flow of 50 mL min^{-1}. Oxygen partial pressure was 6 kPa. The electrochemical cells were placed under a 50 mL min^{-1} flow of helium during initial heating to limit the formation of chemical oxides. CV measurements were carried out with PARSTAT 2263 potentiostat with PowerSuite software package (Princeton Applied Research) at 350 °C and a scan rate of 20 mV s^{-1}.

The charge of each peak generated in a cyclic voltammogram can be used to calculate the moles of species involved in the reaction. For this, a baseline is selected in the cyclic voltammogram, and the total charge determined (Eq. 1). From this, the moles can be tabulated using Faraday's law, given by Eq. 2.

$$Q_i = \frac{\Delta E \sum i}{N\nu} \quad (1)$$

$$\frac{n}{A} = \frac{Q_i}{zF}, \quad (2)$$

where Q_i is the charge density associated with process i; ΔE is the total electrical potential range of the peak; $\sum i$ is the sum of the measured currents densities subtracted from a baseline, ampere per centimeter, for N data points given for a scan rate of ν, volt per second; z is the number of electrons exchanged per mole of oxidized atomic silver; n is the number of moles of oxides formed, and A is the geometric area over which they are formed, centimeter squared. The result is expressed as a mole of oxides produced per geometric surface area of electrode.

Results and discussion

SEM analysis of Ag/YSZ

Figure 1 shows the SEM micrograph of silver films deposited on YSZ before and after thermal treatment. As-deposited 100 nm silver film is continuous and dense (Fig. 1a), while after pretreatment at 550 °C in air and electrochemical polarization at 350 °C in oxygen environment (P_{O2}<20 kPa), this film dewet and form an array of discontinuous nanoparticles/islands (Fig. 1b). Increase in the film thickness results in greater film stability and formation of stable electronically percolated films, shown in Fig. 1c for an 800-nm film after polarization at 350 °C. The effect of film thickness dependence on the thermal stability of films was investigated using in-situ resistance measurements during heating as discussed in the section below.

Percolation studies of silver films

Since an electronically percolated network is required for polarization experiments, determination of the critical thickness was achieved using in-situ resistance measurements with a simple two-electrode system during silver deposition. The critical thickness of a film is the thinnest at which an electronically percolated network is formed. Figure 2 shows the change in electrical resistance of thin silver films as a function of film thickness during deposition. As the film transitions from isolated islands to percolated network, there is a decrease in the resistance [34–36] as shown in Fig. 2. Measured at a constant deposition rate of 0.5 nm s^{-1}, the critical thickness of silver films deposited on polycrystalline YSZ was found to be

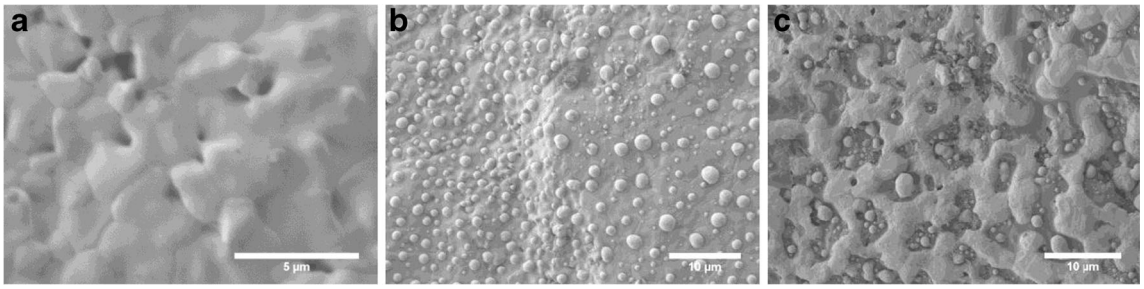

Fig. 1 SEM of Ag/YSZ: **a** as-deposited 100 nm silver film; **b** 100 nm silver film after polarization experiments at 350 °C; and **c** 800 nm silver film after polarization experiments at 350 °C

5.4±0.4 nm when the resistance data is fit to a percolation relation in Eq. 3 [37]:

$$R\sim(p-p_c)^{\mu} \tag{3}$$

However, since metal thin films on oxides are generally unstable or metastable, thermally induced restructuring is common [48]. When sufficiently heated, polycrystalline films undergo simultaneous coarsening and dewetting. Since dewettting involves atomic transport, the rate of dewetting is strongly temperature and film thickness dependant [13, 38]. The microstructure of heat-treated thin films was found to be a function of initial thickness of the film, annealing temperature, and annealing time [13].

Figure 3 shows the in-situ resistance change in thin films of various thicknesses as they undergo heat treatment. The results in Fig. 3 confirm the thickness-dependence of the thermal stability of films. For films thinner than 370 nm, loss of percolation occurs during the pretreatment stage reflected in a sudden increase in resistance. At a thickness higher than 600 nm, the increase in resistance during the pretreatment is less pronounced and remained stable up to 49.5 h (not shown in Fig. 3). The percolation threshold of silver was shown to be 5.4 nm in as-deposited films on YSZ, but silver only formed thermally stable, electronically percolated networks above 500 nm at 350 °C with an hour pretreatment at 550 °C in air. For this reason, an 800-nm silver film was deposited and found to be stable under the pretreatment conditions and during polarization tests.

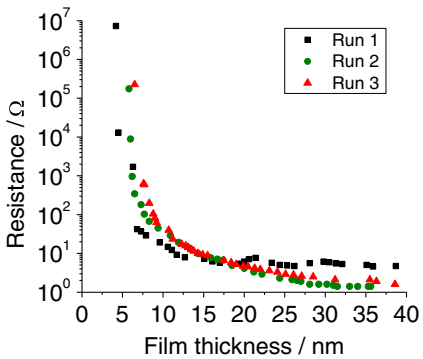

Fig. 2 In-situ resistance measurements of silver during deposition at a rate of 0.5 nm s^{-1}

On the microstructure map developed by Simrick et al., recently, 800 nm silver films deposited on a single crystal YSZ heated at 550 °C had microstructures dominated by a mix of percolated networks and grain growth with small hole formation [13]. Imaging of the film studied in the current work (Fig. 1c) shows greater film porosity after heat treatment than those described by Simrick et al. This increase in porosity can be attributed to the application of small electrical currents required to make in-situ resistance measurements. The effect of electromigration of metal interconnects is well documented in silver [39]: with the application of an electrical current, a discontinuity in electrical conductivity is observed at ambient temperatures in integrated circuits from the electrically driven migration of metal ions. Taking this into consideration, tracking changes to the film microstructure with in-situ resistance techniques at as opposed to ex-situ imaging techniques may result in distortion of findings. Given that the application of such electrochemically percolated thin films interfaced with YSZ requires the application of small currents, it is worthwhile to investigate the effect of changing the applied current on the final microstructure of the film.

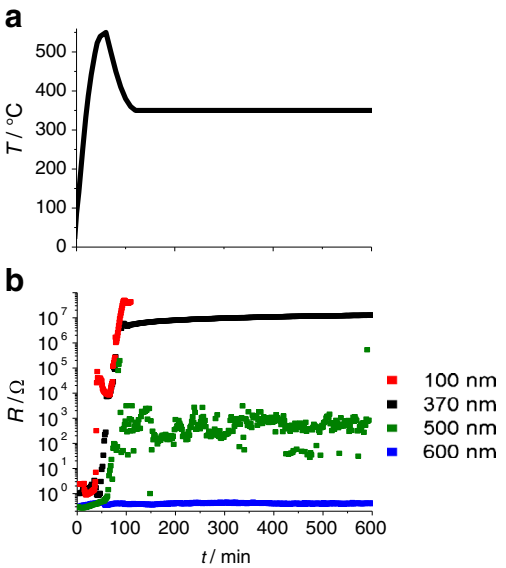

Fig. 3 Effect of film thickness on the thermal stability of thin silver films **a** temperature profile **b** change in film resistance with time

XPS of Ag/YSZ before and after electrochemical measurements

Figure 4 shows the XPS measurements for 100 nm silver samples before and after polarization experiments at 350 °C at P_{O2}=6 kPa. The lower XPS survey spectrum of Fig. 4a was obtained on as-deposited Ag/YSZ. According to it, only Ag, C, and O are present on the surface as expected since the as-prepared Ag layer is continues and dense. The analysis of the O1s peak (Fig. 4c) shows the existence of three peaks around 530.7, 532.1, and 533.4 eV. In the literature, there is a debate concerning the origin of the peak at around 530.5 eV (BE) in the case of Ag-based samples. Surface science studies using XPS and TPD have shown that treatment of polycrystalline silver foils with O_2 and/or CO_2 causes the evolution of a peak at 530.5–530.7 eV [40, 41]. On the other hand, Bao et al. have attributed this peak to bulk oxygen [42]. Thus, this O1s peak can be assigned to chemisorbed oxygen, while the existence of C1s component at around 287 eV (not shown here) implies that this component can be also related to oxygen atoms of chemisorbed CO on the Ag layer. The other two O1s peaks are due to hydroxyl groups and residual water present on the surface [43, 44]. To this point, we should mention that the analysis of O1s does not reveal the existence of a component at ~529.5 eV that in the literature has been attributed to surface oxygen atoms in Ag_2O [45]. The Ag3d XPS peak (Fig. 4e) is detected at 368.3 eV and exhibits a full width at half maximum (FWHM) of 0.65 eV ($Ag3d_{5/2}$). The position and the FWHM of the $Ag3d_{5/2}$ peak clearly indicates that silver is at the metallic state [46].

XPS measurements were performed also after the electrochemical studies over Ag/YSZ sample in order to record changes in the surface composition (Fig. 4 upper spectra). The XPS wide scan (Fig. 4b) shows that on the surface beyond the existence of carbon, oxygen, and silver, yttrium and zirconium are also detected. This finding strongly shows that high temperature and polarization caused significant dewetting of the silver layer and formation of porous layer thus revealing the substrate (YSZ), in accordance with SEM observations. The above finding is further supported by the O1s and Ag3d spectra. The O1s peak (Fig. 4d) exhibits about three times higher intensity, while its analysis reveals the existence of three components at 529.6, 531.2, and at 532.2 eV. The component at the lower BE is attributed to the lattice oxygen atoms in the mixed oxide of YSZ [47], while the component at 531.2 eV is attributed to the chemisorbed oxygen $O^{\delta-}$ on the catalyst surface [48]. The component at the highest BE is due to OH species present on the surface [48]. Additionally, it has been attributed to chemisorbed O^{2-} species in other mixed oxides [49]. The Ag3d peak (Fig. 4f) on the other hand shows a peak intensity decrease of around 65 %. This change is attributed to the fact that the silver layer demonstrates a significant dewetting with uncovered areas of the substrate and a significant loss of its uniformity. The peak is now detected at 368.4 eV ($Ag3d_{5/2}$), while its FWHM has increased to 0.85 eV showing a broadening of about 0.2 eV. This peak broadening is attributed to the fact that the morphology of silver layer has changed and is not homogeneous anymore but it also implies a change of the chemical environment of the silver atoms. This change may be explained by the stronger interaction of silver atoms in the porous nanostructured Ag film with the yttrium and zirconium atoms in YSZ and/or by the changes in the oxidation state of Ag as a result of polarization, as shown below.

Solid electrolyte cyclic voltammetry of Ag/YSZ

Electrochemical polarization of this film can be used to determine the mechanism of oxygen interaction with polarized films commonly used in a variety of electrochemical

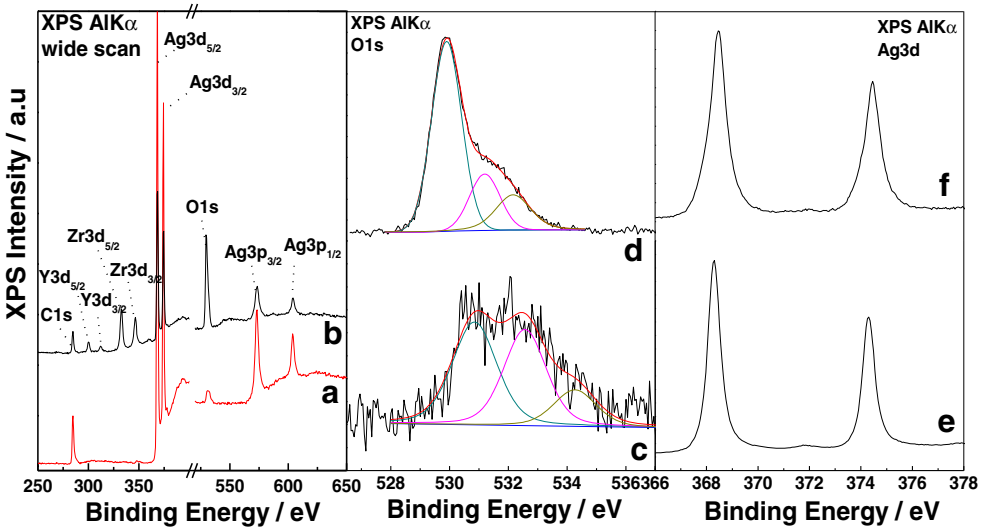

Fig. 4 XPS survey scan of Ag/YSZ before **a** and after polarization experiments at 350 °C **b**, O1s (**c** before and **d** after) and Ag3d (**e** before and **f** after)

applications. The size and locations of peaks on a solid state cyclic voltammogram can provide information about the anodic and cathodic processes occurring at the electroactive interfaces of the electrode.

Figure 5 shows a typical cyclic voltammogram of an 800 nm Ag thin film interfaced with YSZ at P_{O2}=6 kPa and T=350 °C with the baseline used for peak charge calculations (Eq. 1) illustrated. There is a cathodic peak, C1, at 0.15 V with a shoulder, C2, at lower electrical potentials and no anodic peaks. Given that chemically formed oxides decompose at temperatures above 189 °C according to the Ellingham diagram [50], the film is assumed to be in the silver metal state (Ag^0) under open circuit conditions at 350 °C. The current increase at 240 mV could be due to first electrochemical formation of Ag_2O (Eq. 4) and then oxygen evolution at the tpb (Eq. 5). The silver oxide is formed by the reaction of Ag with back-spillover of O^{2-} from the YSZ at the tpb according to Eq. 4. This oxide could grow further inward electrochemically from the three-phase boundary, forming bulk Ag_2O according to Eq. 6:

$$2Ag + O^{2-}(YSZ) \rightleftarrows Ag_2O_{tpb} + 2e^- \quad (4)$$

$$O^{2-}_{ysz} \rightleftarrows \frac{1}{2}O_2 + 2e^- \quad (5)$$

$$Ag_2O_{tpb} \rightleftarrows Ag_2O_{bulk} \quad (6)$$

The electrochemically formed Ag_2O is subsequently reduced in peak C1 and shoulder C2.

Figure 6 shows the effect of positive potential on the formation of Ag_2O. In this experiment, the upper potential limit, E_i, was varied (Fig. 6a), and the changes in electrochemical peak charge (Fig. 6b) were calculated using Eq. 1. Additionally, peak potential (Fig. 6d) and peak current (Fig. 6c) were determined for the stable cycle (3rd cycle). With starting points, E_i, below 400 mV, neither peak C1 or C2 are observed. Above E_i=400 mV, a small cathodic peak at 120 mV appears, followed by a shoulder appearing at more negative potentials

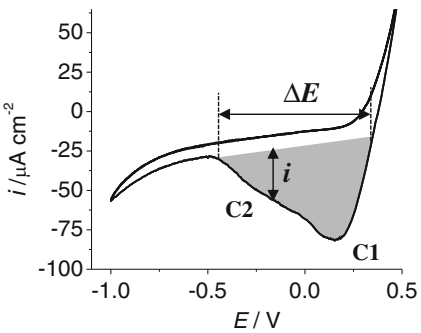

Fig. 5 Cyclic voltammogram of Ag (800 nm)/YSZ, T=350 °C, v=20 mV s^{-1}, P_{O2}=6 kPa

when the anodic hold potential is higher than 700 mV. This potential controlled change in the reduction peaks is an indication that these oxide species are electrochemically formed during the anodic scan in O_2 evolution reaction region.

Additionally, as shown in Fig. 6b, with increased positive potential, there is an exponential increase in the electrochemical peak charge indicating an increase in oxides formed at higher starting potentials. With increased oxide formation, a shift in the peak potential is expected when a passivating scale inhibits the formation of subsequent oxides, as was found for anodic formation of bulk Ag_2O in aqueous systems [51]. In Fig. 6d, for scans beginning below 900 mV, the opposite is observed with the peak C1 shifting slightly to more positive potentials, which is representative of a faster reduction process [52]. Above 900 mV, the scale begins to inhibit the electrochemical reduction. With increased positive potential, the oxide may propagate from tpb within the bulk of the electrode and more negative potentials are required to reduce Ag_2O. According to Faraday's law (Eq. 2), the moles of oxide in the monolayer can be calculated from the total electrochemical charge of the cathodic peak and lies between 1.53 nmol cm^{-2} (900 mV) and 2.83 nmol cm^{-2} (1,000 mV).

Figure 7 shows the effect of changing the scan rate on the CV of silver films with aims at determining the kinetics of these processes. With increasing scan rate, there is an increase in peak current (Fig. 7b) and a shift in the peak potential to more negative values (Fig. 7c). The relation of peak current is linear with respect to $v^{0.5}$, which is consistent with a diffusion limited processes according to the Randles-Sevcick equation [52]. Furthermore, the change in scan rate is linear with the natural logarithm of the scan rate and agrees with Eq. 7, which describes the irreversible reduction of an adsorbed electroactive species [52].

$$\Delta V_{WR} = -\left(\frac{RT}{\alpha_C n_C F}\right)\Delta \ln(v) \quad (7)$$

Figure 8 illustrates the effect of hold time at the positive potential on the first scan of the CV. The changes in the curve as a result of this modification can be used to glean the mechanism of electrochemical oxide formation. Two regions of behavior can be observed in this data. The first region, at hold times below 60 s, is characterized by an increase in peak current and a shift in peak potential to more negative values as hold time is increased, shown in Fig. 8b and c, respectively. During this stage, initial current is constant at an average of −163 μA cm^{-2} and is consistent with the formation of passivating oxide layer, though there is insufficient data to conclude whether the mechanism follows a

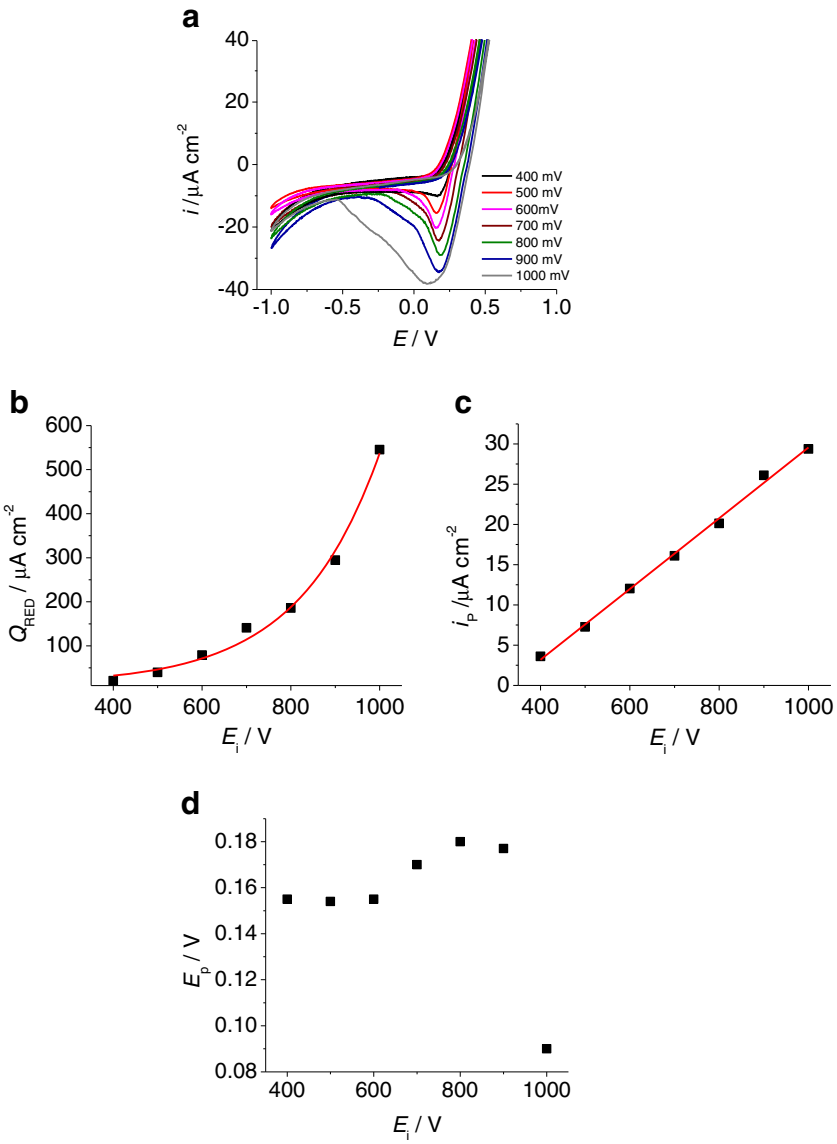

Fig. 6 Effect of positive potential on **a** cyclic voltammogram of Ag (800 nm)/YSZ, P_{O2}=6 kPa, third cycle, T=350 °C, v=20 mV s^{-1}; **b** charge of reduction process; **c** peak current density; and **d** peak potential

parabolic or logarithmic growth mode. Above 60 s, there is a drop in initial current and a shift to more positive peak potentials. The total anodic charge expended at the beginning of the first scan which accounts for processes given by Eqs. 3–5 above can be used to determine the current efficiency based on the reduction of silver oxides during the negative sweep, according to Eqs. 8 and 9.

$$\eta_{Ag_2O} = \frac{Q_{AN}}{Q_{Ag_2O}} \times 100 = \frac{i_i t_h}{Q_{C1} + Q_{C2}} \times 100 \quad (8)$$

$$\eta_{o_2} = 100 - \eta_{Ag_2O} \quad (9)$$

where i_i is the current density value measured following the hold time, t_H and Q_{AN} are the charge measured during t_H, and Q_{Ag_2O} is the charge associated with the reduction of Ag_2O which is equal to the sum of Q_{C1} and Q_{C2}, the charge measured from peaks C1 and C2 as labeled in Fig. 2. Calculating the current efficiency of the reduction of silver oxides (η_{Ag_2O}) and that of oxygen evolution (η_{O_2}) can give an indication of the efficiency of the electrode. The result is shown in Fig. 8c, at low hold times, current efficiencies for the formation of silver oxides is high, but decreases significantly due to the inhibiting nature of Ag_2O scale.

Proposed model

Figure 9 illustrates a proposed model for the silver oxide growth in Ag/YSZ based on the experimental

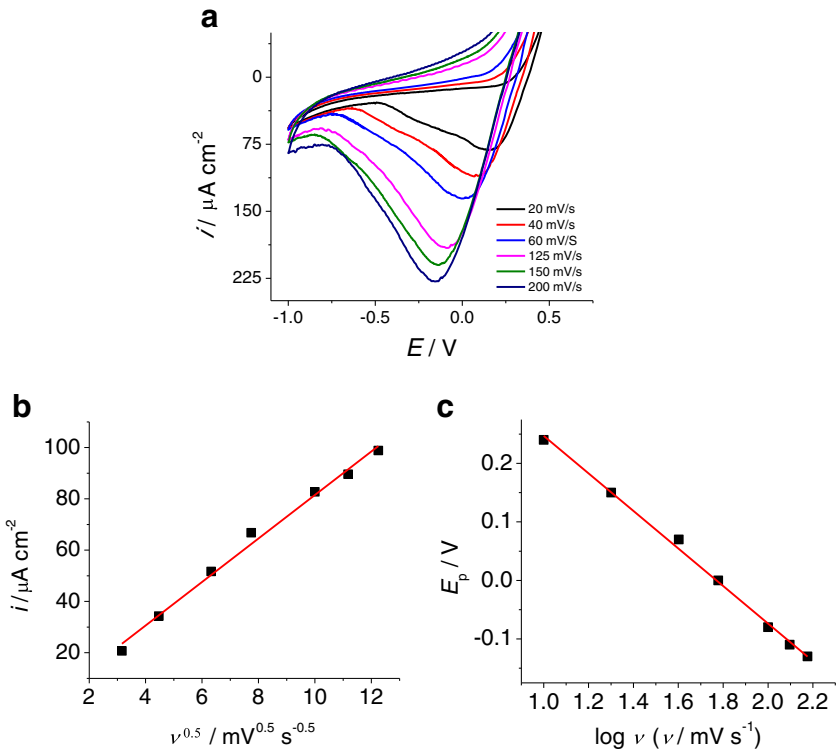

Fig. 7 Effect of scan rate on **a** cyclic voltammogram of Ag (800 nm)/YSZ, Conditions *idem* and scan rates indicated in the figure; **b** peak current; and **c** peak potential

results discussed above. In the literature, models for the O_2,Me/YSZ system behavior based on cyclic voltammetry studies have been presented where Me is a metal electrode composed of nickel [29], palladium

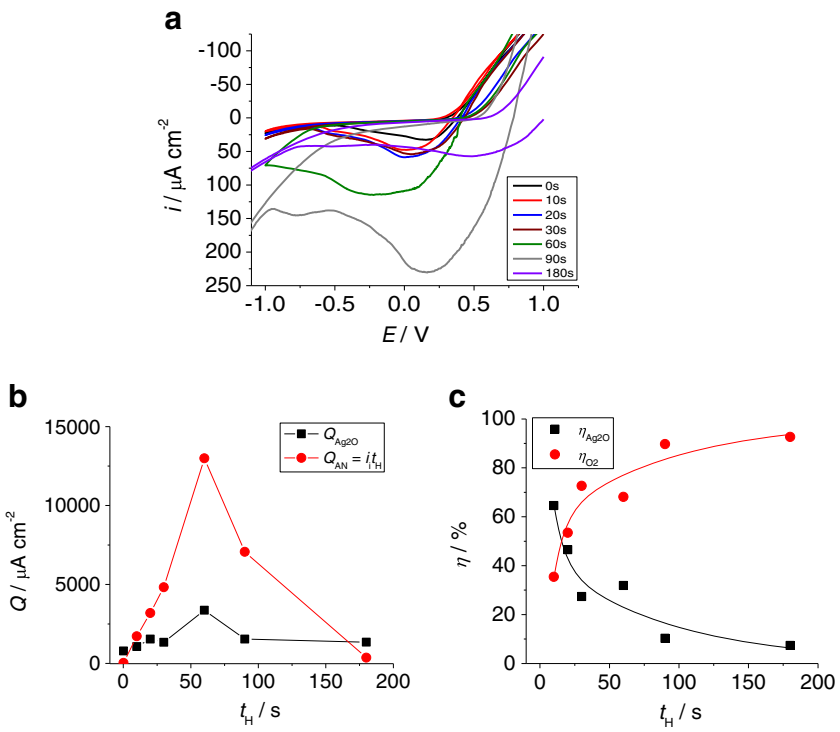

Fig. 8 Effect of hold time at 1,000 mV for **a** cyclic voltammogram of Ag (800 nm)/YSZ, Conditions *idem*; **b** charge of anodic and cathodic processes (explanation in the text); and **c** current efficiencies from Eqs. 8 and 9

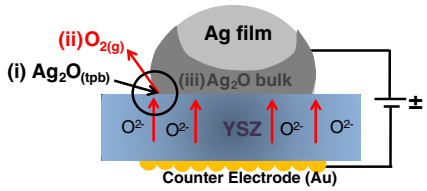

Fig. 9 Model of electrochemical oxide formation on 800 nm silver film interface with YSZ

[30], or platinum [28] thin films. The model shown in Fig. 9 is discussed in relation to these studies.

At open circuit potential, the electrode is assumed to be in the metal state, and upon application of an external positive potential, two processes are proposed to occur: Ag_2O formation and oxygen evolution at the three-phase boundary, as shown in Fig. 9 process i and ii, respectively. With increasing initial positive potentials, the oxide is driven into the bulk of the electrode (Fig. 9, process iii). The electrochemical formation of silver oxides at the tpb and within the bulk of the electrode is reflected in the cyclic voltammogram as the presence of a cathodic peak (C1) and a shoulder (C2) which was sensitive to changes in the starting anodic potential of the CV. The presence of multiple adjacent cathodic peaks is also reflected in findings of Falgairette et al., who found these to be representative of location specific oxides formed at longer polarization times for sputtered 880 nm nickel films on YSZ [28]. The back-spillover of O^{2-} from the YSZ may occur along the three-phase boundary, at the two-phase boundary of electrode and YSZ, or may migrate through existing scale to form bulk oxides [28]. Based on the behavior of silver electrodes in aqueous alkaline systems [53] and the high oxygen mobility within silver [13], the formation of bulk silver oxide is proposed. By contrast, the platinum model presents a submonolayer to single monolayer formation of oxides along the tpb which propagates along the interface between Pt and YSZ upon higher polarization times [28]. This is due to the low oxygen solubility in platinum if compared with silver.

With increased starting anodic potential, the total charge of silver oxides present is also found to increase logarithmically, while these oxides become more difficult to reduce (shift in cathodic peak potential to more negative potentials) due to the presence of a passivating surface layer extending from the three-phase boundary, as was found in nickel sputtered films [29]. With increased initial hold time at a given anodic potential, there is an observed decrease in current efficiency for Ag_2O reaction resulting from oxide buildup over the electroactive tpb. With change in scan rate, the silver behavior was found to be in agreement with Randles-Sevcick equation for diffusion limited irreversible processes.

Conclusion

Evaporative PVD was used to deposit high purity silver thin films on YSZ. Using an in-situ resistance technique during deposition, percolated network began to form at a critical thickness of 5.4±0.4 nm. However, when these films were heat pretreated at 350 °C in air, as confirmed using SEM and XPS measurements, the films were found to dewet from the substrate (YSZ) and form non-percolated nanoparticles/islands which resulting in loss of polarization of the film. The thermal stability of silver films on polycrystalline YSZ was found to be thickness dependent, and films greater than 600 nm were found to be necessary to produce stable films. A film of 800 nm showed a continuous network and was selected for electrochemical studies by means of cyclic voltammetry.

XPS measurements of 100 nm Ag/YSZ before and after polarization at 350 °C, P_{O2}=6 kPa showed that for as-prepared sample, only Ag, C, and O are present on the surface. The position and the FWHM of the Ag3d peak indicated that silver is at the metallic state. For the sample after polarization, the XPS wide scan showed in addition to C, O, and Ag, also yttrium and zirconium peaks. This finding confirmed that high temperature and polarization caused a significant dewetting of the silver and formation of porous layer. At the same time, the Ag3d peak showed a peak intensity decrease of around 65 % and FWHM broadening as a result of dewetting and a loss of film uniformity, as well as due to a change of the chemical environment of Ag atoms.

Solid electrolyte cyclic voltammetry was used to investigate 800 nm Ag film on polycrystalline YSZ. Studies have illustrated the formation of Ag_2O with positive polarization from the electrochemically back-spillover O^{2-} species from the YSZ support. The interpretation of the results of this study has led to the presentation of the following model. Under anodic polarization, there are two processes that take place simultaneously at tpb: formation of Ag_2O and O2 evolution. With prolonged application of a positive electrical potential, Ag_2O oxide was found to propagate from the tpb inside the Ag film along the two-phase boundaries. The accumulation of this scale resulted in electrode resistance and loss of current efficiency for Ag_2O process, such that the oxygen evolution reaction becomes favored.

Acknowledgments Financial support from the Natural Science and Engineering Research Council (NSERC), Canada is gratefully acknowledged.

References

1. Shim JH, Kim YB, Park JS et al (2012) Patterned silver nanomesh cathode for low-temperature solid oxide fuel cells. J Electrochem Soc 159:B541–B545
2. Stoukides M (2000) Solid-electrolyte membrane reactors: current experience and future outlook. Catal Rev 42(1&2):1–70
3. Riegel J, Neumann H, Wiedenmann H (2002) Exhaust gas sensors for automotive emission control. Solid State Ionics 152–153: 783–800
4. Bebelis S, Karasali H, Vayenas C (2008) Electrochemical promotion of CO2 hydrogenation on Rh/YSZ electrodes. J Appl Electrochem 38:1127–1133
5. Baranova EA, Thursfield A, Brosda S et al (2005) Electrochemical promotion of ethylene oxidation over Rh catalyst thin films sputtered on YSZ and TiO_2/YSZ Supports. J Electrochem Soc 152:E40–E49
6. Vernoux P, Gaillard F, Bultel L et al (2002) Electrochemical promotion of propane and propene oxidation on Pt/YSZ. J Catal 208:412–421
7. Dow W-P, Huang T-J (1996) Yttria-stabilized zirconia supported copper oxide Catalyst II. Effect of oxygen vacancy of support on catalytic activity for CO oxidation. J Catal 160:171–182
8. Munoz M, Gallego S, Beltran J, Cerda J (2006) Adhesion at metal–ZrO2 interfaces. Surf Sci Rep 61:303–344
9. Vernoux P, Lizzaraga L, de Lucas-Consuegra A et al (2013) Ionically conducting ceramics as active catalyst supports. Chem Rev 113: 8192–8260
10. Dole H, Isaifan JR, Sapountzi FM et al (2013) Low temperature toluene oxidation over Pt nanoparticles supported on yttria stabilized-zirconia. Catal Lett 143:996–1002
11. Krishnamurthy R, Yoon Y, Srolovitz D, Car R (2004) Oxygen diffusion in yttria-stabilized zirconia: a new simulation model. J Am Ceram Soc 87:1821–1830
12. Cantos-Gómez A, Ruiz-Bustos R, Van Duijn J (2011) Ag as an alternative for Ni in direct hydrocarbon SOFC anodes. Fuel Cells 11:140–143
13. Simrick NJ, Kilner JA, Atkinson A (2012) Thermal stability of silver thin films on zirconia substrates. Thin Solid Films 520:2855–2867
14. Chongterdtoonskul A, Schwank JW, Chavadej S (2012) Effects of oxide supports on ethylene epoxidation activity over Ag-based catalysts. J Mol Cat A 358:58–66
15. Verykios X, Stein FP, Coughlin RW (1980) Influence of metal crystallite size and morphology on selectivity and activity of ethylene oxidation catalyzed by supported silver. J Catal 66:368–382
16. Kenson RE, Lapkin M (1970) Kinetics and mechanism of ethylene oxidation: reactions of ethylene and ethylene oxide on a silver catalyst. J Phys Chem 74:1493–1502
17. Bernhardt TM (2005) Gas-phase kinetics and catalytic reactions of small silver and gold clusters. Int J Mass Spectrom 243:1–29
18. Aoyama N, Yoshida K, Abe A, Miyadera T (1997) Characterization of highly active silver catalyst for NOx reduction in lean-burning engine exhaust. Catal Lett 43:249–253
19. Baiker A, Kilo M, Maciejewskiq M et al (1993) Hydrogenation of CO2 over copper, silver and gold-zirconia catalyst: comparative study of catalyst properties and reaction pathways. New Frontiers in Catalysis. pp 5071–5080
20. Seimanides S, Stoukides M (1984) Solid-electrolyte-aided study of methane oxidation. J Catal 88:490–498
21. Li N, Gaillard F (2009) Catalytic combustion of toluene over electrochemically promoted Ag catalyst. Appl Catal B 88:152–159
22. Gaillard F, Li N (2009) Electrochemical promotion of toluene combustion on an inexpensive metallic catalyst. Catal Today 146: 345–350
23. Yi J, Yentekakis IV, Vayenas CG (1994) Potential programmed reduction—a new technique for investigating the thermodynamics and kinetics of chemisorption on catalysis supported on solid electrolytes. J Catal 148:240–251
24. Vayenas CG, Bebelis S, Brosda S et al (2002) Electrochemical promotion of catalysis promotion, electrochemcial promotion and metal support interactions. Kluwer Academic Publishers, New York
25. Wagner C (1970) Adsorbed atomic species as intermediates in heterogeneous catalysis. In: 21 (ed) Adv. Catal. Academic Press Inc., London, pp 323–378
26. Vayenas CG, Ioannides A, Bebelis S (1991) Solid electrolyte cyclic voltammetry for in situ investigation of catalyst surfaces. J Catal 129: 67–87
27. Jaccoud A, Foti G, Comninellis C (2006) Electrochemical investigation of platinum electrode in solid electrolyte cell. Electrochim Acta 51:1264–1273
28. Falgairette C (2010) Stored electrogenerated promoters inducing sustainable enhanced Pt catalyst activity. Sciences-New York 4690: 230
29. Souentie S, Falgairette C, Comninellis C (2010) Electrochemical investigation of the O2(g), Ni/YSZ system using cyclic voltammetry. J Electrochem Soc 157:P49
30. Jiménez-Borja C, Souentie S, González-Cobos J et al (2013) Electrochemical investigation of O_2-exposed Pd electrodes supported on YSZ. J Appl Electrochem 43:417–424
31. Mutoro E, Luerssen B, Günther S, Janek J (2009) The electrode model system Pt(O_2)|YSZ: Influence of impurities and electrode morphology on cyclic voltammograms. Solid State Ionics 180: 1019–1033
32. De Lucas-Consuegra A, Dorado F, Jiménez-Borja C et al (2009) Use of potassium conductors in the electrochemical promotion of environmental catalysis. Catal Today 146:293–298
33. Briggs D, Seah MP (1996) Practipuis, vol. 1, 2nd edn. Wiley, New York
34. Angadi M, Udachan A (1981) Electrical properties of thin nickel films. Thin Solid Films 79:149–153
35. Kirkpatrick S (1973) Percolation and conduction. Rev Mod Phys 45: 574–588
36. Neugebauer CA, Webb MB (1962) Electrical conduction mechanism in ultrathin, evaporated metal films. J Appl Phys 33:74–82
37. Essam J (1980) Percolation theory. Rep Prog Phys 43:834–912
38. Thompson CV (2012) Solid-state dewetting of thin films. Annu Rev Mater Res 42:399–434
39. Wu K, Bradley RM (1994) Theory of electromigration failure in polycrystalline metal films. Phys Rev B 50:12468–12488
40. Bukhtiyarov V, Kondratenko V, Boronin AI (1993) Features of the interaction of a CO + O_2 mixture with silver under high pressure. Surf Sci Lett 293:L826–L829
41. Bukhtiyarov V, Boronin A, Savchenko V (1994) Stages in the modification of a silver surface for catalysis of the patrial oxidation of ethylene. I Action of Oxygen. J Catal 1502:262–267
42. Boa X, Muhler M, Pettinger B et al (1993) On the nature of the active state of silver during catalystic oxidation of methanol. Catal Lett 22: 215–225
43. Ntais S, Dracopoulos V, Siokou A (2004) $TiCl_4$(THF)2 impregnation on a flat SiO_x/Si(1 0 0) and on polycrystalline Au foil: Determination of surface species using XPS. J Mol Cat A 220: 199–205
44. Palloukis F, Zafeiratos S, Jaksic M, Neophytides SG (2004) The chemical state of electrodeposited thin Cr films on a polycrystaline Ni foil. J New Mater Electrochem Syst 7:173–177
45. Zemlyanov DY, Savinova E, Scheybal A et al (1998) XPS observation of OH groups incorporated in an Ag(111) electrode. Surf Sci 418:441–456
46. Huang W, Jiang Z, Dong F, Bao X (2002) An AES, XPS and TDS study on the growth and property of silver thin film on the Pt(1 1 0)-(1×2) surface. Surf Sci 514:420–425

47. Majumdar D, Chatterjee D (1991) X-ray photoelectron spectroscopic studies on yttria, zirconia, and yttria-stabilized zirconia. J Appl Phys 70:988
48. Bae JS, Park S-S, Mun BS et al (2012) Surface modification of yttria-stabilized-zirconia thin films under various oxygen partial pressures. Thin Solid Films 520:5826–5831
49. Xu Q, Huang D, Che W et al (2004) X-ray photoelectron spectroscopy investigation on chemical states of oxygen on surfaces of mixed electronic–ionic conducting La0.6Sr0.4Co1−yFeyO3 ceramics. Appl Surf Sci 228:110–114
50. Harriott P (1971) The oxidation of ethylene using silver on different supports. J Catal 21:56–65
51. Burstein GTN, Newman RC (1980) Anodic behaviour of scratched silver electrodes in alkaline solution. Electrochim Acta 25:1009–1013
52. Bard AJ, Faulkner LR (2001) Electrochemical methods - fundamentals and applications, 2nd Ed. 864
53. Abd El Rehim SS, Hassan HH, Ibrahim MAM, Amin MA (1998) Electrochemical behaviour of a silver electrode in NaOH solutions. Monatsh Chem 129:1103–1117